Journal of Physics: Conference Series **688** (2016) 012055 doi:10.1088/1742-6596/688/1/012055

Shock Hugoniot measurements of CH at Gbar pressures at the NIF

A. L. Kritcher[1], T. Doeppner[1], D. Swift[1], J. Hawreliak[1], J. Nilsen[1], J. Hammer[1], B. Bachmann[1], G. Collins[1], O. Landen[1], C. Keane[1], S. Glenzer[2], S. Rothman[3], D. Chapman[3], D. Kraus[4], R.W.Falcone[4]

[1]Lawrence Livermore National Laboratory, Livermore, CA, [2]SLAC Accelerator National Laboratory, Menlo Park, CA, USA,[3]Atomic Weapons Establishment, Reading, United Kingdom, [4]Department of Physics, University of California Berkeley, Berkeley, CA, USA

E-mail: kritcher2@llnl.gov

Abstract. Laboratory measurements of the shock Hugoniot at high pressure, exceeding several hundred Mbar, are of great importance in the understanding and accurate modeling of matter at extreme conditions. In this work we present a platform to measure the material properties, specifically the single shock Hugoniot and electron temperature, at extreme pressures of ∼Gbar at the National Ignition Facility (NIF). In these experiments we launch spherically convergent shocks into solid CH, using a Hohlraum radiation drive. X-ray radiography is applied to measure the shock speed and infer the mass density profile, enabling determining of the material pressure and Hugoniot equation of state. X-ray scattering is applied to measure the electron temperature through measurement of the electron velocity distribution.

1. Introduction

Shock Hugoniot measurements of matter at high energy density are important for understanding the structure and evolution of gas-giant planets [1, 2, 3] or highly evolved stars [4]. At Gbar pressures atomic shell effects [5] may come into play which can change the predicted compressibility at given pressure due to pressure and temperature ionization. In addition, benchmarking dense matter models in the regime that is relevant for fusion energy experiments, which assemble material to the highest densities and pressures ever achieved in the laboratory [6, 7] (hundreds of g/cc and >100 Gbar) is important. Previous experiments have reached Gbar conditions via underground nuclear explosions [8]. Near Gbar conditions have also been observed in x-ray driven colliding Au foils [9]. In these experiments, the shock Hugoniot was not directly measured and potential preheat of the target foil could significantly impact interpretation of the results. More recent experiments have reached Gbar pressures in laser driven cone-in-shell targets, but had issues with shock uniformity and stability, resulting in a non ideal platform for a detailed Equation of State (EOS) measurement [10].

We create Gbar conditions in the laboratory using high-energy lasers at the National Ignition Facility (NIF) [11] and present a stable platform well suited for shock Hugoniot measurements. In these experiments we drive a strong convergent shock wave through solid spherical targets in an indirectly driven laser geometry and characterize the Hugoniot and electron temperature using x-ray radiography [12, 13, 14] and x-ray Thomson scattering [15, 16, 17, 18, 19, 20, 21, 22]. We measure the mass density profile and shock speed from the radiographic signal, and infer

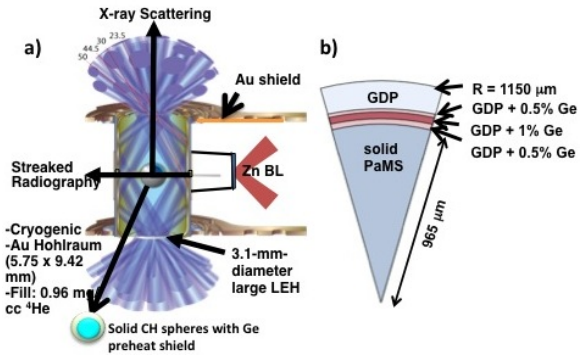

Figure 1. a) Schematic of the experimental setup. Here solid targets of CH are shock compressed using a indirectly driven hohlraum radiation source. The plasma is probed with x-ray radiography in the equatorial direction and x-ray scattering in the polar direction. b) Wedged cross-section of the solid PaMS target with a Ge doped GDP (Glow Discharge Polymer) ablator.

the pressure in the shocked region using the Hugoniot relations. In these experiments preheat of the interior of the target does not have a strong impact on interpretation of the results. The calculated preheat due to absorption of Au Mband radiation from the Hohlraum is less than 1eV, which is a small perturbation to the total pressure. In the following sections, we will present experiments at the NIF to employ these techniques, under an accepted NIF basic science shot-time allocation.

2. Experimental Setup and Method

In these experiments we launch a strong shock wave into a solid ball of polystyrene using a Hohlraum radiation drive. This radiation drive is created using 184 laser beams that heat gold Hohlraum walls and create a black body cavity at radiation temperatures of up to 280 eV. The Au wall motion due to heating and expansion is mitigated by filling the Hohlraum with 0.96 mg/cc of He^4. We track the shock wave traveling through the target via streaked x-ray radiography as a function of radius and time. The x-ray radiography backlighter is created via laser irradiation of a Zn foil mounted outside of the Hohlraum. Two slits at the waist of the hohlraum enable transmission of the backlighter photons to the target and to the x-ray streak camera in the equatorial direction. The same backlighter photons are also used for x-ray Thomson scattering in the polar direction. An Au shield is used to block the direct line of sight of the backlighter photons to the scattering spectrometer in the polar direction. See Fig.1 a) for a schematic of the experimental configuration. The solid targets consist of a 965μm radius solid sphere of PAMS (Poly(Alpha-MethylStyrene)), covered by a graded doped Ge preheat shield, Fig.1 b). The preheat shield is used to mitigate pre-heating of the PAMS by Hohlraum Au M-band emission.

The time-resolved x-ray radiography will be used to measure the shock speed u_s and mass density ρ profiles. Rankine-Hugoniot relations relate the pressure P and density $\rho = 1/\nu$ in the shocked state to the unshocked material (subscript 0), given u_s, $P = u_s^2\rho_0(1 - \rho_0/\rho)$. Thus, by measuring ρ and u_s we infer the pressure and constrain the shock Hugoniot. The calculated error bars on this measurement are about 4.5% in both density and pressure. In addition we measure x-ray Thomson scattering from free electrons, or Compton scattering. The Compton feature, downshifted in energy, provides information on the electron velocity distribution through Doppler broadening. If the plasma is non-degenerate, probing the velocity distribution through

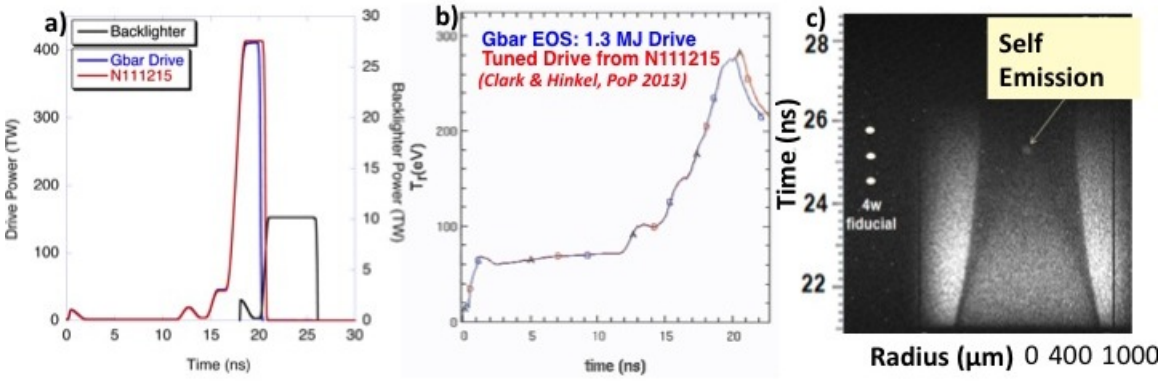

Figure 2. a) Power profiles vs time of the laser drive (red/blue) and backlighter beams (black). b) Radiation temperature as a function of time, derived from integrated Hohlraum simulations for post shot N111215 (red) and the modified Gbar EOS drive (blue). c) Simulated radiograph using the Gbar 1.3 MJ radiation drive.

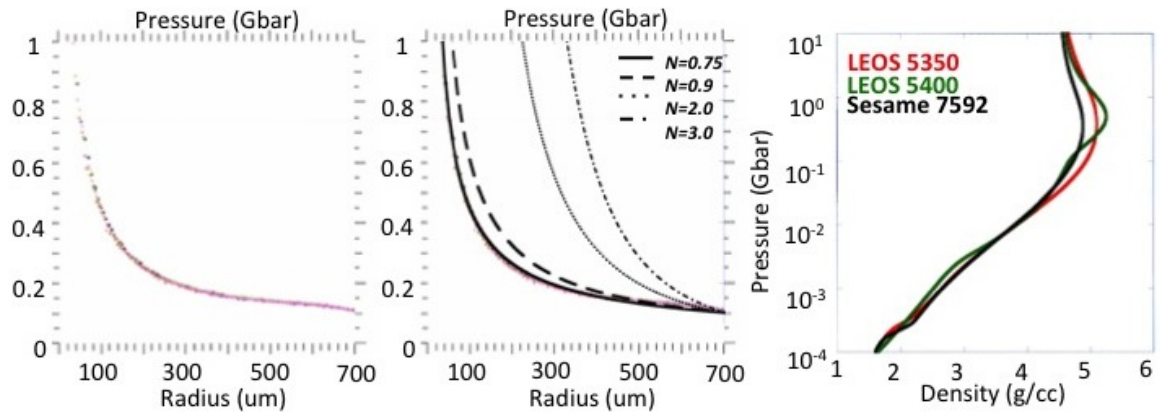

Figure 3. (Left hand side) Pressure at the shock front as a function of shock front radius, using LEOS 5350 (red/magenta), LEOS 5400 (green) and Sesame 7592(black). (Right hand side) The same plot as on the left hand side, with analytical expressions of the pressure increase as a function of radius, where $P = P_0(r_0/r)^N$.

measurement of the Compton feature width, provides a measure of the electron temperature.

3. Radiation Hydrodynamic Simulations

Radiation hydrodynamic simulations have been preformed using the code HYDRA [23] in capsule-only simulations that use a frequency dependent radiation drive surrounding capsule. The radiation drive is derived from integrated Hohlraum simulations which includes the non-Planckian behavior of the hohlraum. We start from a radiation drive, derived from experiment N111215, that has been tuned in a post-shot manner [24] to match experimental observables in ICF implosions for a similar laser pulse shape. This radiation drive was modified to account for using eight of the drive beams to irradiate the backlighter foil. The radiation drive is also adjusted for using a laser drive energy of 1.3 MJ in the first experiments, compared to 1.45 MJ for shot N111215, see Fig.2 b).The corresponding laser power profiles and radiation temperatures as a function of time are shown in Fig.2 a) and b). Also shown is the backlighter power profile

as a function of time, which is delayed from the drive beams to capture the shock convergence at the target center. A simulated radiograph, as a function of radius and time, including realistic noise and backlighter functions shows that we can resolve the shock front down to small radii, of <100 μm, see Fig. 3 a).

The simulations have been performed using three choices of Equations of State (EOS) models LEOS 5350 (GDP), LEOS 5400 (GDP), and Sesame 7592 (polystyrene) and tabular OPAL opacities [25]. Figure 3 (left hand side) shows the predicted pressure as a function of radius using LEOS 5350 and 5400, Sesame 7592 and the radiation drive shown in see Fig.2 b). Reaching Gbar pressures in a planar shock wave geometry is currently not feasible at the NIF for the mm scale samples required to employ diagnostics such as x-ray radiography. Therefore, we employ a sphericaly convergent shock wave geometry where convergent flow increases the shock pressure. These simulations show that we can reach near Gbar pressures in this platform using a 1.3 MJ Hohlraum radiation drive.

The pressure in a converging spherical shock wave increases as the radius decreases, and can be approximated by [26],

$$P \propto r^{-2\beta} \tag{1}$$

where $\beta^{-1} = 1/2 + 1/\gamma + (\gamma/2(\gamma-1))^{1/2}$ is an approximation for strong shock waves and γ is the adiabatic index. For $\gamma = 5/3$, $\beta = 0.45$ and for $\gamma = 4/3$, $\beta = 0.375$. The increase in pressure due to convergence is smaller than for a sound wave because the shock wave is non-isentropic with a fraction of the energy being dissipated into heat. This analytical relationship is shown in the center plot of Fig.2 b), over-plotted on the simulated curves. Here the pressure, P, is a function of the initial pressure, P_0, radius, r, and initial radius, $r + 0$: $P = P_0(r_0/r)^N$. For the solid curve $N = 0.75$, the dashed curve $N = 0.9$, the dotted curve $N = 2$, and the dash dot curve $N = 3$. Here, we see that the curve with $N = 0.75$, and $\beta = 4/3$, best fits the simulated pressure increase, which may be influenced by radiative preheat of the shock front at high convergence ratios. Measurement of the shape of the mass density profile will provide indication on the onset of radiative preheat at the shock front. The pressure as a function of radius is weakly dependent on choice of equation of state. However, the compressibility of the material at a given pressure is strongly dependent on choice of EOS this can be seen on the right hand side of Fig.3 for the three choices of EOS models considered. Since we will be measuring both the density and pressure simultaneously, we can benchmark these EOS models.

In summary, we have developed a platform to create and probe matter at Gbar pressures at the NIF. In these experiments we measure the shock speed, mass density profile, and infer the pressure, thereby constraining the single shock Hugoniot of samples at pressures of 100Mbar-Gbar. In addition, experimental measurement of the pressure increase as a function of radius can provide information on the adiabatic index. This work was performed under the auspices of the U.S. Department of Energy by Lawrence Livermore National Laboratory under Contract No. DE-AC52-07NA27344 and supported by Laboratory Directed Research and Development Grant No. 13-ERD-073.

References

[1] L. Stixrude, Phys. Rev. Lett. **108**, 055505 (2012).
[2] S. Seager, M. Kuchner , C. A. Hier-Majumder, and B. Militzer, Astrophys. J. **669**, 1279 (2007).
[3] D.C. Swift, J. Eggert, D.G. Hicks, S. Hamel, K. Caspersen,*et al.* Astrophys. J. 744, 59 (2012)
[4] V. Fortov, Extreme States of Matter: On Earth and in the Cosmos, 224 (2011).
[5] J. C. Pain, High En. Den. Phys., **3** 204 (2007).
[6] J. Nuckolls *et al.*, Nature, **239** (1972).
[7] J. D. Lindl *et al.*, Phys. Plasmas **11**, 339. (2004).
[8] Vladimirov AS, Voloshin NP, Nogin VN, Petrovtsev AV, Simonenko VA., Sov Phys - JETP Lett **39** (1984).
[9] R. Cauble, Phys. Rev. Lett. **70**, 14 (1993).

[10] K. Shigemori *et al.*, Appl. Phys. Lett. **102**, 183501. (2013).
[11] E. I. Moses, R. N. Boyd, B. A. Remington, C. J. Keane, and R. Al-Ayat, Phys. Plasmas **16**, 041006 (2009).
[12] D. G. Hicks, B. K. Spears, D. G. Braun, R. E. Olson, *et al.*, Rev. Sci. Instrum. **81**, 10E304 (2010).
[13] D. G. Hicks, N. B. Meezan, E. L. Dewald, A. J. Mackinnon, *et al.*,Phys. Plasmas 19, 122702 (2012)
[14] D. C. Swift, J. A. Hawreliak, *et al.*, Proc. American Physical Society, CP1426 pp.477-480 (2011).
[15] S. H. Glenzer and Ronald Redmer, Rev. Mod. Phys. **81**, 1625 (2009).
[16] A. L. Kritcher, T. Doeppner, C. Fortmann, T. Ma,*et al.* , Phys. Rev. Lett. **107**, 015002 (2011).
[17] A. L. Kritcher, Paul Neumayer,John Castor,Tilo Dppner,*et al.*, Science, **322**, 69 (2008).
[18] L. B. Fletcher, A. Kritcher, A. Pak, T. Ma, T. Dppner,*et al.*,Phys. Plasmas 20, 056316 (2013)
[19] G. Gregori, S. H. Glenzer, K. B. Fournier, K. M. Campbell,*et al.*, Phys. Rev. Lett. **101**, 045003 (2008).
[20] H. J. Lee, P. Neumayer, J. Castor, T. Dppner, R. W. Falcone, *et al.*,, Phys. Rev. Lett. **102**, 115001 (2009).
[21] B. Barbrel, M. Koenig, A. Benuzzi-Mounaix, E. Brambrink, *et al.*,, Phys. Rev. Lett. **102**, 165004 (2009).
[22] D. Riley, N. C. Woolsey, D. McSherry, I. Weaver, A. Djaoui, and E. Nardi , Phys. Rev. Lett. **84**, 1704 (2000).
[23] M. Marinak, S. W. Haan, T. R. Dittrich, R. E. Tipton, and G. B. Zimmerman, Phys. Plasmas **5**, 1125 (1998).
[24] D. S. Clark,D. E. Hinkel, D. C. Eder1, O. S. Jones, S. W. Haan, *et al.*,, Phys. Plasmas 20, 056318 (2013).
[25] C. A. Iglesias and F. J. Rogers, Astrophys. J. 464, 943 (1996).
[26] F. Winterberg, *The Rel. of Thermonuclear En. by Inertial Confinement*, World Scientific Publishing (2010).